Detecting Entanglement Structure in Continuous Many-Body Quantum Systems

Philipp Kunkel,[1,*] Maximilian Prüfer,[1] Stefan Lannig,[1] Robin Strohmaier,[1] Martin Gärttner,[1,2,3] Helmut Strobel,[1] and Markus K. Oberthaler[1]

[1]*Kirchhoff-Institut für Physik, Universität Heidelberg, Im Neuenheimer Feld 227, 69120 Heidelberg, Germany*
[2]*Physikalisches Institut, Universität Heidelberg, Im Neuenheimer Feld 226, 69120 Heidelberg, Germany*
[3]*Institut für Theoretische Physik, Universität Heidelberg, Philosophenweg 16, 69120 Heidelberg, Germany*

(Received 21 May 2021; accepted 6 December 2021; published 10 January 2022)

A prerequisite for the comprehensive understanding of many-body quantum systems is a characterization in terms of their entanglement structure. The experimental detection of entanglement in spatially extended many-body systems describable by quantum fields still presents a major challenge. We develop a general scheme for certifying entanglement and demonstrate it by revealing entanglement between distinct subsystems of a spinor Bose-Einstein condensate. Our scheme builds on the spatially resolved simultaneous detection of the quantum field in two conjugate observables which allows the experimental confirmation of quantum correlations between local as well as nonlocal partitions of the system. The detection of squeezing in Bogoliubov modes in a multimode setting illustrates its potential to boost the capabilities of quantum simulations to study entanglement in spatially extended many-body systems.

DOI: 10.1103/PhysRevLett.128.020402

Entanglement between spatial regions of isolated quantum systems is at the heart of phenomena such as eigenstate thermalization [1,2] and many-body localization [3,4]. Spatial entanglement has been experimentally assessed in small systems with discrete degrees of freedom, such as spins or few particle systems [5–8]. These methods rely on the experimental capability of preparing and maintaining pure states as well as detection on the single-particle level. These requirements are exceedingly hard to fulfill in generic situations in nature where many particles interact and the system is described by continuous quantum fields. Here we show that the spatially resolved joint measurement of noncommuting field quadratures allows certifying entanglement in these situations with no assumptions about the purity of the global state.

Our experimental platform is a spin-1 Bose-Einstein condensate (BEC), where spin mixing leads to squeezing in the conjugate spin-1 operators $\hat{S}_x$ and $\hat{Q}_{yz}$ [9]. To open a more general perspective on entanglement in continuous many-body quantum systems, we define the quantum field $\hat{\Phi} = \hat{S}_x - i\hat{Q}_{yz}$. For our experiments, we initially prepare a BEC of ^{87}Rb atoms in the magnetic substate $m_F = 0$ of the $F = 1$ hyperfine manifold in a spatially one-dimensional situation [see Fig. 1(a)]. This corresponds to the vacuum state of the quantum field $\hat{\Phi}(y)$. By a controlled energy shift of $m_F = 0$ we initiate spin-mixing dynamics. This leads to squeezing of the field quadratures $(\hat{\Phi}^\dagger + \hat{\Phi})/2$ and $(\hat{\Phi}^\dagger - \hat{\Phi})/2i$ and to the buildup of entanglement between spatial subsystems [10–12]. We directly sample the phase-space distribution of the quantum field via a joint measurement of the two field quadratures, $\hat{S}_x$ and $\hat{Q}_{yz}$. For this,

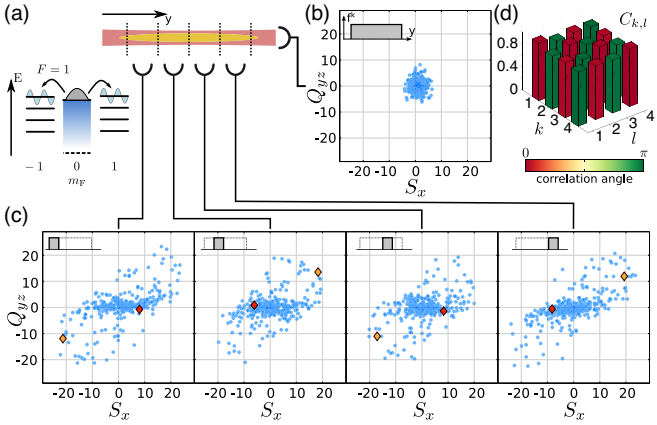

FIG. 1. Sampled phase-space distributions of global and local observables. (a) Schematics of the level scheme for the physical preparation of the target state and of the longitudinally expanded atomic cloud. The initially populated $m_F = 0$ level is tuned (shading) close to resonance with the third excited eigenmode in $m_F = \pm 1$ via off-resonant microwave dressing. In the right-hand part, the dashed lines indicate the evaluation regions with a length of 20 μm each. Panels (b) and (c) show the sampled phase-space distributions for the global observables and for the local subsystems, respectively. The corresponding partitioning functions are shown in the insets. The state has been prepared by 800 ms of spin-mixing dynamics which results in a non-Gaussian distribution in the local partitions. The red and yellow points highlight single experimental realizations illustrating the strong correlations between the individual subsystems. These correlations strongly suppress the fluctuations of the global observables leading to a Gaussian distribution as shown in (b). Panel (d) shows a quantitative analysis of the first-order coherence between different subsystems revealing strong anticorrelations between neighboring partitions.

we couple the $F = 1$ hyperfine manifold to $F = 2$ which serves as an ancillary system (see Refs. [13,14] for details). After inducing spin rotations via radio frequency fields, we measure in each experimental realization the populations of the magnetic substates in the $F = 1$, 2 manifolds, from which we estimate the expectation values $S_x(y)$ and $Q_{yz}(y)$, respectively. This estimation can be done with high precision, since approximately 600 atoms contribute on average to the signal at each position y after integrating over the transversal directions and the spatial resolution of 1.3 μm.

In the following, we will show that accessing the local as well as the global phase-space distributions is a key ingredient for entanglement detection. Entanglement is defined as inseparability of the quantum state with respect to specific partitions of the system. Given the spatial resolution of our imaging we are able to analyze general partitions via

$$\Phi_k = \mathcal{N}_k \sum_y f^k(y)\Phi(y), \tag{1}$$

where the functions f^k can represent a partitioning in separate spatial regions as well as in mode functions, e.g., Bogoliubov modes. Both types will be used in the following. The normalization $\mathcal{N}_k$ is chosen such that the corresponding operators fulfill the commutation relation $[\hat{\Phi}_k, \hat{\Phi}_k^\dagger] = 2$. This normalization is possible, since we detect the commutator of the observables $\hat{S}_x$ and $\hat{Q}_{yz}$ [for the connection to the detected particle numbers in $F = 1$ and $F = 2$, see Supplemental Material (SM) [14]].

Our readout scheme gives us access to the phase-space distribution in any partition and the direct sampling allows analyzing correlations between them. To demonstrate this capability, we tune the spin-mixing process into resonance with the third excited mode of the external potential [21,22] and let the system evolve for 800 ms [see Fig. 1(a)]. Prior to imaging, we switch off the longitudinal confinement to let the atomic cloud expand by a factor of 4 to an extension of about 80 μm. The corresponding phase-space distribution of the global observables, i.e., $f^k(y) = 1$, is shown in Fig. 1(b), which features an isotropic Gaussian distribution.

In Fig. 1(c) we show the phase-space distributions for a local analysis corresponding to the partitioning functions as indicated in the insets. These distributions are highly non-Gaussian and characterized by large fluctuations. In conjunction with the observed small fluctuations in the global observables shown in Fig. 1(b), this implies strong correlations between the spatial subsystems. To reveal the structure of the correlations present we evaluate the first-order coherence,

$$C_{k,l} = \frac{\langle \Phi_k^* \cdot \Phi_l \rangle}{\sqrt{\langle |\Phi_k|^2 \rangle \cdot \langle |\Phi_l|^2 \rangle}}, \qquad k, l \in \{1\text{–}4\}, \tag{2}$$

where $\langle \cdot \rangle$ indicates the average over all experimental realizations. $C = |C|e^{i\theta}$ is in general a complex quantity where the absolute value $|C|$ quantifies correlations between the local fields and the relative angle between the fluctuations of the local fields is given by θ. In Fig. 1(d) we find θ to be changing by π between neighboring subsystems demonstrating strong anticorrelations as expected from the spatial structure of the populated third excited mode. That these correlations are found in any phase-space orientation can be seen explicitly in the examples shown in Fig. 1(c), where two realizations in orthogonal phase-space directions are highlighted in red and yellow.

In the following we will show that knowledge of correlations between quantum fields in different partitions can be used to certify entanglement. For this, we tune the spin-mixing dynamics such that the two energetically lowest trap modes are squeezed as shown in Fig. 2(a). We choose an evolution time of 100 ms in the squeezing regime. Microscopically this corresponds to a mean number of 32 atoms in the magnetic substates ± 1 compared to the initial BEC of 4×10^4 atoms. In order to experimentally confirm the expected squeezing of the phase-space distribution in each mode, we choose the partitions indicated in the insets of Fig. 2(b). The corresponding elliptical phase-space distributions are shown in the upper row of Fig. 2(b). We compare the standard deviations of the data with the ones expected for the vacuum state as indicated by the blue and black lines, respectively. We find for both partitions fluctuations below the classical limit, where the maximally squeezed orientations are marked by red lines. This confirms the squeezing in the two modes. Because of the energy difference between the two modes, the relative orientation $\Delta\Theta_S$ of the two squeezing directions evolves dynamically when switching off the microwave dressing of $m_F = 0$. Employing different hold times we prepare $\Delta\Theta_S \approx 0°$ and 90°.

For a quantitative analysis of the squeezing level the photon shot noise, readout splitting, and technical noise that contribute to the measured signal have to be taken into account. For the data shown in Fig. 2 we find after subtracting the photon shot noise contribution minimal fluctuations of 0.7 ± 0.1. The vacuum fluctuations of the ancillary states limit the level of fluctuations to 0.5 for a perfectly squeezed state. Taking those into account leads to an inferred squeezing of -3 dB. For reaching this detection limit the off-resonant excitations during the splitting pulses have to be suppressed to a level of smaller than 10^{-5}.

Strikingly, even though both spatial modes feature squeezing for the two situations with $\Delta\Theta_S \approx 0°$ and 90° the spatial entanglement structure differs. For a relative orientation of 0° the local phase-space distributions shown in the lower row of Fig. 2(b) are similar to the ones found within the mode partitions and also feature fluctuations below the classical limit. In contrast, for an angle of 90° the

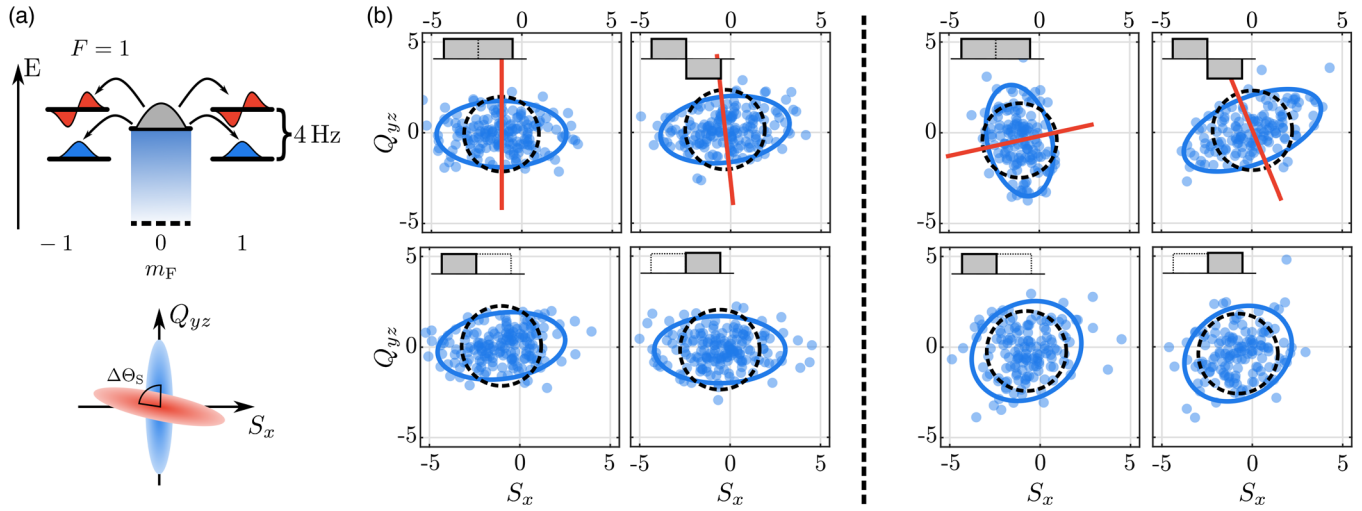

FIG. 2. Superposition of two squeezed vacuum states. (a) Illustration of simultaneous spin mixing in two spatial modes (blue and red). The initially populated $m_F = 0$ level is tuned (shading) close to resonance with two energetically lowest eigenmodes in $m_F = \pm 1$ via off-resonant microwave dressing (upper part). This results in simultaneous squeezing in the two modes with relative squeezing angle $\Delta\Theta_S$ (lower part). (b) Phase-space distributions for different partitioning functions as indicated in the insets of each panel. We prepare two different relative squeezing angles of $\Delta\Theta_S \approx 0°, 90°$ which are shown in the left-hand and right-hand part, respectively. The blue ellipses show the 2 s.d. interval of the distribution and the black dashed circles show the fluctuations expected for the initial vacuum state (including photon shot noise). The upper row reveals the squeezing in the individual modes, where the red lines indicate the axis of smallest fluctuations. In the case of $\Delta\Theta_S \approx 0°$ we find squeezing in the local partitions while for $\Delta\Theta_S \approx 90°$ the fluctuations are increased along all directions compared to the vacuum state (lower row).

local distributions exhibit enhanced fluctuations exceeding those of the vacuum state. Since this analysis corresponds to a partial trace over the complement of the respective subsystem, finding increased fluctuations in the remaining system is an indication of spatial entanglement.

In order to rigorously show the presence of entanglement we derive an entanglement witness $\mathcal{W}$ [23] for the experimentally realized joint measurements. Our measurement strategy allows extracting the field component along arbitrary orientations θ via $F_k(\theta) = \mathrm{Re}(\Phi_k^\dagger e^{-i\theta})$ with $k \in \{L, R\}$ from the sampled local phase-space distributions, where Re() denotes the real part. These quantities allow us to evaluate the following criterion fulfilled for all separable states [24]:

$$\mathcal{W} = \Delta^2 u(\theta_L, \theta_R) + \Delta^2 u(\theta'_L, \theta'_R) - [|\sin(\Delta\theta_L)| + |\sin(\Delta\theta_R)|] \geq 0, \quad (3)$$

where $u(\theta_L, \theta_R) = [F_L(\theta_L) + F_R(\theta_R)]/\sqrt{2}$ and $\Delta\theta_k = \theta_k - \theta'_k$. Here, $|\sin(\Delta\theta_k)|$ accounts for the bound of the local uncertainty relation and assumes equal atom numbers in the two partitions (for the imbalanced case, see SM [14]). Since the local observables are determined in joint measurements the bound has been adapted with respect to its original form [24] by exploiting this knowledge about the measurement process [25,26]. The fluctuations in $u(\theta_L, \theta_R)$ quantify the degree of correlation between the subsystems and $\mathcal{W} < 0$ signals the presence of entanglement.

From the sampled phase-space distributions we evaluate the variances $\Delta^2 u(\theta_L, \theta_R)$ for any pair of angles. Figure 3(a) shows that for the two relative squeezing angles shown in Fig. 2 we observe pronounced minima where the fluctuations are suppressed below the atomic shot noise

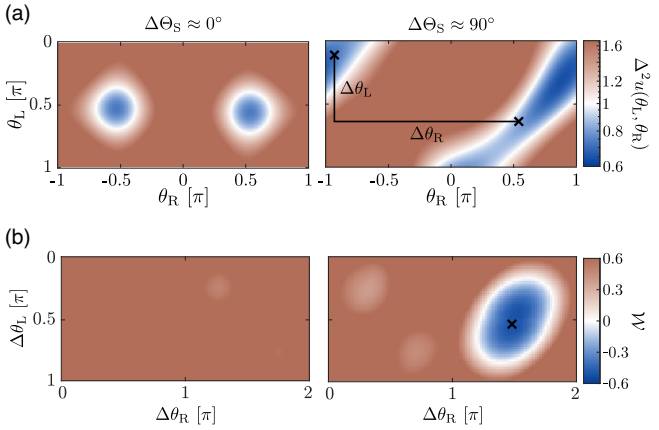

FIG. 3. Witnessing entanglement between subsystems. (a) Fluctuations in the observable u quantifying correlations between the subsystems as a function of the local field projection angles, θ_L and θ_R. Here, the blue regions signal fluctuations below the atomic shot noise limit. While for $\Delta\Theta_S = 0°$ (left) we observe fluctuations for specific angle pairs, the continuous diagonal band of reduced fluctuations seen for $\Delta\Theta_S = 90°$ (right) is what allows witnessing entanglement. (b) Entanglement witness as a function of local relative angles, where the blue regions signal entanglement. For each pair of local relative angles, we minimized the first line of Eq. (3). The point of minimal $\mathcal{W}$ is indicated by the black cross. The corresponding pair of local orientations is indicated in (a).

limit ($\Delta^2 u = 1$). We find a violation of Eq. (3) by minimizing $\mathcal{W}$ over all pairs of analysis angles. As the last term in Eq. (3) only depends on the relative angles $\Delta\theta_k$, we minimize the variances with respect to θ_k for each choice of $\Delta\theta_k$. The resulting values of $\mathcal{W}$ are shown in Fig. 3(b), where regions of $\mathcal{W} < 0$ are visible. For the case that the squeezing ellipses in the two modes have the same orientation, i.e., $\Delta\Theta_S = 0°$ [see Fig. 2(b)], we find that the witness does not flag entanglement between the left and right half, although the phase-space distributions of both halves feature squeezing. For $\Delta\Theta_S = 90°$ our witness detects entanglement consistent with the enhanced fluctuations in the local partitions shown in Fig. 2(b). In this case, we find for the witness a minimal value of -0.51 ± 0.14 for $\Delta\theta_L = 0.53\pi$ and $\Delta\theta_R = 1.45\pi$, where we subtracted the independently characterized photon shot noise contribution of 0.13 (see SM [14]). We also find entanglement between the two halves for different relative orientations of the squeezing ellipses, e.g., $\Delta\Theta_S = 45°$ (see SM [14]).

Having established the experimental capabilities of our method, we now turn to a multimode situation which is the interesting regime for quantum simulation of many-body systems. Here, we study the quantum structure of multiple spatial modes in a boxlike trapping potential (see Fig. 4). We confine the atoms to the central part of a weak harmonic trapping potential (with longitudinal and transversal trap frequencies of $2\pi \times 1.5$ Hz and $2\pi \times 170$ Hz, respectively)

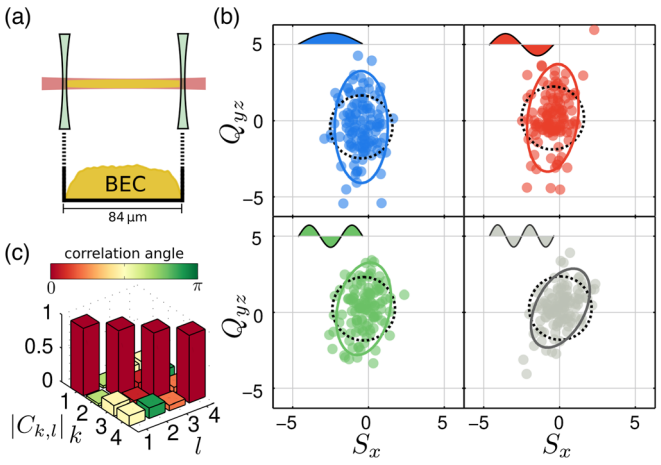

FIG. 4. Simultaneous vacuum squeezing of multiple Bogoliubov modes. (a) Schematic of a boxlike trapping potential implemented by combining an elongated attractive harmonic dipole potential (red) with two repulsive barriers (green). The detected BEC density is shown in the lower part (yellow). (b) Sampled phase-space distributions for the partitionings indicated in the insets, which reveal vacuum squeezing in the four energetically lowest Bogoliubov modes. The colored solid lines indicate the 2 s.d. interval of the distribution and the dashed black lines show the fluctuations expected for the initial vacuum state including photon shot noise. (c) $C_{k,l}$ for the data shown in (b). This confirms the independence of the individual Bogoliubov modes as expected in the low depletion limit.

by adding two repulsive barriers which are spaced by 84 μm. This leads to a flat atomic density as shown in Fig. 4(a). The spin interaction strength of 1.2 Hz allows us to vacuum squeeze different spatial modes simultaneously since the energy difference between the ground and third excited mode of the box potential is only 1.2 Hz.

Our experimental observations directly reveal the squeezing in the individual Bogoliubov modes by taking them as partitioning functions $f^k(y)$ [see Fig 4(b) insets]. For a single realization we evaluate the field in mode k according to Eq. (1). Experimentally, we find squeezing for the four lowest spatial modes by examining the phase-space distributions at 100 ms evolution time [see Fig. 4(b)]. The widths of the distributions (shown as colored ellipses) are smaller than expected for the initially prepared vacuum state (black circle) and amount to a maximal inferred squeezing of -8 dB for the third excited mode.

From the fluctuations along the antisqueezed axis we infer a mean number of less than 6 atoms in each Bogoliubov mode. Compared to the overall atom number of $\sim 3 \times 10^4$ this correspond to a regime of low depletion where the Bogoliubov approximation is valid. In this regime uncorrelated squeezing dynamics of each mode is expected [27]. We explicitly confirm that these modes are independent by evaluating the first-order coherence $C_{k,l}$ [see Eq. (2)] between the individual partitions as shown in Fig. 4(c). This highlights a major advantage of our detection scheme as extracting these coherences would be experimentally challenging and resource intensive with sequential projective measurements. There mode-selective spin rotations as well as a large number of relative analysis angles would be required.

We present a very general strategy to extract correlations between various partitions of the system as well as their entanglement structure. This lays the ground for resolving the role of entanglement in different phenomena such as thermalization of isolated quantum systems [28], the emergence of hydrodynamics, and quantum effects in gravity with analog quantum simulators [29]. Since our entanglement detection scheme is model independent it may be employed for certifying quantum operation of an analog simulator, a task that is indispensable when exploring phenomena beyond the reach of classical devices [30].

We thank Thorsten Zache for valuable comments on the manuscript and Monika Schleier-Smith, Luca Pezzè, Stefan Floerchinger, and Jürgen Berges for discussion. This work is supported by ERC Advanced Grant Horizon 2020 EntangleGen (Project-ID 694561), the Deutsche Forschungsgemeinschaft (DFG, German Research Foundation) under Germanys Excellence Strategy EXC2181/1-390900948 (the Heidelberg STRUCTURES Excellence Cluster), within the Collaborative Research Center SFB1225 (ISOQUANT, Project-ID 273811115), and by the Baden-Württemberg Stiftung gGmbH. P. K. acknowledges support by the Studienstiftung des deutschen Volkes.

*fieldentanglement@matterwave.de

[1] L. DAlessio, Y. Kafri, A. Polkovnikov, and M. Rigol, Adv. Phys. **65**, 239 (2016).

[2] J. M. Deutsch, Rep. Prog. Phys. **81**, 082001 (2018).

[3] R. Nandkishore and D. A. Huse, Annu. Rev. Condens. Matter Phys. **6**, 15 (2015).

[4] D. A. Abanin, E. Altman, I. Bloch, and M. Serbyn, Rev. Mod. Phys. **91**, 021001 (2019).

[5] J. Smith, A. Lee, P. Richerme, B. Neyenhuis, P. W. Hess, P. Hauke, M. Heyl, D. A. Huse, and C. Monroe, Nat. Phys. **12**, 907 (2016).

[6] A. Lukin, M. Rispoli, R. Schittko, M. E. Tai, A. M. Kaufman, S. Choi, V. Khemani, J. Léonard, and M. Greiner, Science **364**, 256 (2019).

[7] T. Brydges, A. Elben, P. Jurcevic, B. Vermersch, C. Maier, B. P. Lanyon, P. Zoller, R. Blatt, and C. F. Roos, Science **364**, 260 (2019).

[8] A. Bergschneider, V. M. Klinkhamer, J. H. Becher, R. Klemt, L. Palm, G. Zürn, S. Jochim, and P. M. Preiss, Nat. Phys. **15**, 640 (2019).

[9] C. D. Hamley, C. S. Gerving, T. M. Hoang, E. M. Bookjans, and M. S. Chapman, Nat. Phys. **8**, 305 (2012).

[10] M. Fadel, T. Zibold, B. Décamps, and P. Treutlein, Science **360**, 409 (2018).

[11] K. Lange, J. Peise, B. Lücke, I. Kruse, G. Vitagliano, I. Apellaniz, M. Kleinmann, G. Tóth, and C. Klempt, Science **360**, 416 (2018).

[12] P. Kunkel, M. Prüfer, H. Strobel, D. Linnemann, A. Frölian, T. Gasenzer, M. Gärttner, and M. K. Oberthaler, Science **360**, 413 (2018).

[13] P. Kunkel, M. Prüfer, S. Lannig, R. Rosa-Medina, A. Bonnin, M. Gärttner, H. Strobel, and M. K. Oberthaler, Phys. Rev. Lett. **123**, 063603 (2019).

[14] See Supplemental Material at http://link.aps.org/supplemental/10.1103/PhysRevLett.128.020402 for experimental details on state preparation, trapping potentials readout sequence, imaging calibration, definition of the relevant operators, summary of the squeezing results, entanglement verification at $\Delta\Theta_S = 45°$, and a detailed derivation of the entanglement witness used in this work, which includes Refs. [15–20].

[15] W. Muessel, H. Strobel, M. Joos, E. Nicklas, I. Stroescu, J. Tomkovič, D. B. Hume, and M. K. Oberthaler, Appl. Phys. B **113**, 69 (2013).

[16] C. F. Ockeloen, A. F. Tauschinsky, R. J. C. Spreeuw, and S. Whitlock, Phys. Rev. A **82**, 061606(R) (2010).

[17] W. M. De Muynck and J. M. V. A. Koelman, Phys. Lett. **98A**, 1 (1983).

[18] C. Branciard, Proc. Natl. Acad. Sci. U.S.A. **110**, 6742 (2013).

[19] M. T. Quintino, T. Vértesi, and N. Brunner, Phys. Rev. Lett. **113**, 160402 (2014).

[20] R. Uola, T. Moroder, and O. Gühne, Phys. Rev. Lett. **113**, 160403 (2014).

[21] M. Scherer, B. Lücke, G. Gebreyesus, O. Topic, F. Deuretzbacher, W. Ertmer, L. Santos, J. J. Arlt, and C. Klempt, Phys. Rev. Lett. **105**, 135302 (2010).

[22] F. Deuretzbacher, G. Gebreyesus, O. Topic, M. Scherer, B. Lücke, W. Ertmer, J. Arlt, C. Klempt, and L. Santos, Phys. Rev. A **82**, 053608 (2010).

[23] O. Gühne and G. Tóth, Phys. Rep. **474**, 1 (2009).

[24] L.-M. Duan, G. Giedke, J. I. Cirac, and P. Zoller, Phys. Rev. Lett. **84**, 2722 (2000).

[25] E. Arthurs and J. Kelly, Bell Syst. Tech. J. **44**, 725 (1965).

[26] U. Leonhardt, P. Knight, and A. Miller, *Measuring the Quantum State of Light*, Cambridge Studies in Modern Optics (Cambridge University Press, Cambridge, England, 1997).

[27] J. D. Sau, S. R. Leslie, M. L. Cohen, and D. M. Stamper-Kurn, New J. Phys. **12**, 085011 (2010).

[28] M. Rigol, V. Dunjko, and M. Olshanii, Nature (London) **452**, 854 (2008).

[29] D. Boiron, A. Fabbri, P.-É. Larré, N. Pavloff, C. I. Westbrook, and P. Ziń, Phys. Rev. Lett. **115**, 025301 (2015).

[30] J. Eisert, D. Hangleiter, N. Walk, I. Roth, D. Markham, R. Parekh, U. Chabaud, and E. Kashefi, Nat. Rev. Phys. **2**, 382 (2020).